fluids

MDPI

Article

Numerical Analysis of Multi-Particulate Flow Behaviour in CFB Riser Coupled with a Kinetic Theory

Fardausur Rahaman [1], Abd Alhamid Rafea Sarhan [2,3,*] and Jamal Naser [2]

[1] SLR Consulting Australia Pty Ltd., Spring Hill, QLD 4000, Australia
[2] Department of Mechanical and Product Design Engineering, Swinburne University of Technology, Hawthorn, VIC 3122, Australia; jnaser@swin.edu.au
[3] Department of Biomedical Engineering, University of Melbourne, Melbourne, VIC 3010, Australia
* Correspondence: asarhan@swin.edu.au

Abstract: In this work, a three-dimensional CFD model for the gas–solid flow of two different particle sizes in a CFB riser coupled with a kinetic theory (KT) has been developed. The properties of the solid phases are calculated using the proposed multi-particle kinetic theory. The CFD model is implemented in the commercial CFD software CFX4.4. In the current model, one gas phase and two solid phases are used. However, the model is generalised for one carrier phase and N number of solid phases to enable a realistic particle size distribution in the system. The momentum, volume fraction and granular temperature equations are solved for each individual solid phase and implemented into the CFD model through user-defined functions (UDFs). The k-ε turbulence model is used in simulating the circulating fluidised bed model. For verification, simulation results obtained with the new KT model were compared with experimental data, and then the model was used for further analysis. It was found that the proposed multi-particle model can be used to calculate the properties of gas–solid systems with particles of different sizes and/or densities, removing the assumptions of previous models that required all the particles to be of an equal mass, size and density.

Keywords: CFD; fluidised granular bed; kinetic theory; multi-particulate flow; CFB riser

Citation: Rahaman, F.; Sarhan, A.A.R.; Naser, J. Numerical Analysis of Multi-Particulate Flow Behaviour in CFB Riser Coupled with a Kinetic Theory. *Fluids* **2023**, *8*, 257. https://doi.org/10.3390/fluids8090257

Academic Editors: Saidul Islam and D. Andrew S. Rees

Received: 26 July 2023
Revised: 30 August 2023
Accepted: 4 September 2023
Published: 21 September 2023

1. Introduction

Gas-fluidised bed reactors are frequently used in many important industrial processes, especially in the oil industry [1–3], mineral processing [4,5] and electric power generation industries [6] due to their excellent heat and mass transfer characteristics, on the one hand, and solid mobility, on the other hand. Despite its widespread application, the hydrodynamics of gas-fluidised beds, unfortunately, remains poorly understood. This lack of understanding poses a significant obstacle to the up-scale of industrially important reactors [7–9]. Computational Fluid Dynamics (CFD) is a powerful tool for gaining a theoretical understanding of the complex multiphase flow and transfer processes in reactors [10–12]. However, CFD has not matured enough to predict the flow behaviour of a gas–solid flow system containing solids of different sizes and densities.

Much progress has been made in recent years towards developing computer codes for describing the hydrodynamics of gas-fluidised beds. Most of the developed models are based on a two-phase description, one gas and one solid phase and all the particles are assumed to have one diameter, density and a coefficient of restitution [13–16]. However, in real particle systems, particles of different sizes and densities exist; furthermore, the operation of many industrial processes is strongly dependent on having different particle sizes in the reactors. For such systems, a multi-particle approach is required for modelling and describing this class of gas–solid flow systems. There are some studies available in the literature [17–20] where different sizes and densities of particles were considered as different phases. However, due to the limitations of their models [3], none of them can be used to predict the behaviour of a multi-particle system. For example, Bell (2000)

and Manger (1996) [17,18] extended the kinetic theory to binary mixtures of solids with unequal granular temperatures for the phases. In these models, fixed viscosities were used for each solid phase, and an interphase momentum transfer term was derived to account for the momentum transfer between solid phases due to collisions. However, arbitrary constants were used in determining the number of collisions. As the number of collisions can be obtained from kinetic theory, the kinetic theory approach would appear to be superior [21,22].

As highlighted earlier, many existing models have been tailored for single-particle flow scenarios [23–29]. Consequently, the capacity to forecast the intricate flow dynamics of particles of varying sizes within a gas–solid flow framework remains a notable deficiency, leading to considerable inaccuracies in the advancement and upscaling of gas–solid flow systems such as fluidised beds. In light of this, the principal objective of this study is to pioneer a multi-particle Computational Fluid Dynamics (CFD) model designed for a Circulating Fluidised Bed (CFB) while scrutinising the intricate flow behaviours of diverse-sized particles. In order to address this gap, the current work leverages the kinetic theory of the model introduced by [3] to simulate the behavior of a CFB riser. This kinetic theory model exhibits its versatility in accommodating multi-particle systems, where variations in particle mass, diameter, restitution coefficient, density and granular temperature are considered. Notably, the model takes into account the heterogeneity of particles and encompasses diverse flow characteristics within solid phases, including solid viscosity, solid pressure, collisional heat flux and bulk viscosity, stemming from intricate particle–particle interactions. For this investigation, the chosen CFB configuration aligns with a previous study conducted by Mathiesen in 1997 [30], thereby establishing a solid foundation for the ensuing analysis.

As previously mentioned, most of the developed models are applicable to a single particle flow system [23–29]. Thus, the ability to predict the flow behaviour of different-sized particles in a gas–solid flow system is still lacking, which causes significant errors in the development and scale-up of gas–solid flow systems such as fluidised beds. Therefore, the main objective of the present study is to develop a multi-particle CFD model for a Circulating Fluidised Bed (CFB) and analyse the flow behaviour of different-sized particles. The kinetic theory model developed by [3] is used in the present work to simulate the CFB riser. This model is applicable to multi-particle systems, where the mass, diameter, restitution coefficient, density and granular temperature of the particles may be unequal. Different flow properties for solid phases (such as solid viscosity, solid pressure, collisional heat flux and bulk viscosity) resulting from particle–particle interactions are obtained from the multi-particle kinetic theory. The CFB that has been selected for investigation was previously tested by Mathiesen (1997) [30].

2. Mathematical Model

Detailed development of the multi-particle kinetic theory, along with mathematical comparison with other available theories in the literature, has been presented in our previous publication [3,21,31]. This theory has been implemented in the commercial CFD software CFX and used to simulate the riser section of a circulating fluidised bed having particles of different sizes. Two different particle species have been considered. Particles of each species are considered smooth, elastic and homogeneous spheres. Different flow properties for solid phases (such as solid viscosity, solid pressure, collisional heat flux and bulk viscosity) resulting from particle–particle interactions are obtained from the multi-particle kinetic theory. Interphase transfer terms (momentum transfer, fluctuating energy transfer) between the solid phases are also added to the code through the user subroutine. In the present model, we employed the standard k-epsilon turbulence model to simulate the experimental results. The choice of this turbulence model was motivated by its widespread use and applicability to a wide range of engineering scenarios. The k-ε model is well-suited for capturing turbulence characteristics and flow phenomena in various configurations, making it a suitable candidate for our investigation. A comparison of predicted results

with experimental results validates the model [32]. The CFB that has been selected for investigation was previously tested by [30]. Details of the governing equations used in the simulations and the model formulation are summarised in Table 1 [3]:

Table 1. Governing equations for gas–solid flow through riser, constitutive law and boundary conditions.

1. The number of binary collisions

$$N_{ij} = \frac{\sqrt{\pi}}{4} d_{ij}^2 n_i n_j g_{ij} \left(\frac{m_i m_j}{\theta_i \theta_j}\right)^{\frac{3}{2}} \times \frac{1}{A^{3/2} D^2} \left[1 + \frac{3\pi B^2}{AD} + \frac{45\pi B^4}{8(AD)^2} \cdots\cdots\right]$$

were coefficients *A*, *B*, *D*:

$$A = \frac{m_i\theta_j + m_j\theta_i}{2\theta_i\theta_j} \quad B = \frac{m_i m_j(\theta_i - \theta_j)}{2m_0\theta_i\theta_j} \quad D = \frac{m_i m_j(m_i\theta_i + m_j\theta_j)}{2m_0^2\theta_i\theta_j}$$

2. The conservation equations

$$\frac{\partial n\langle\psi_i\rangle}{\partial t} + \nabla.\left(n_i < \boldsymbol{c}_i\psi_i > + \sum_j P_{c,ij}\right) = < n_i F_i \frac{\partial \psi_i}{\partial \boldsymbol{c}} > + N_{c,ij}$$

Collisional stress contribution:

$$P_{c,ij} = -\frac{1}{2} d_{ij}^3 \int\limits_{c_{ij}.k>0} (\psi_i' - \psi_i) \boldsymbol{c}_{ij}.\boldsymbol{k}\boldsymbol{k} f_{ij}^{(2)}\left(\boldsymbol{r} - \frac{1}{2} d_{ij}\boldsymbol{k}, \boldsymbol{c}_i, \boldsymbol{r} + \frac{1}{2} d_{ij}\boldsymbol{k}, \boldsymbol{c}_j\right) d\boldsymbol{k} d\boldsymbol{c}_i d\boldsymbol{c}_j$$

$$N_{c,ij} = \frac{1}{2} d_{ij}^2 \int\limits_{c_{ij}.k>0} \left(\psi_j' + \psi_i' - \psi_j - \psi_i\right) \boldsymbol{c}_{ij}.\boldsymbol{k} f_{ij}^{(2)}\left(\boldsymbol{r} - \frac{1}{2} d_{ij}\boldsymbol{k}, \boldsymbol{c}_i, \boldsymbol{r}, \boldsymbol{c}_j\right) d\boldsymbol{k} d\boldsymbol{c}_i d\boldsymbol{c}_j$$

Conservation of mass for species i:

$$\frac{\partial}{\partial t}(n_i m_i) + \nabla.(n_i m_i v_i) = 0$$

Volume fraction of species i:

$$\varepsilon_i = \frac{n_i m_i}{\rho_i}$$

Conservation of momentum of species i:

$$\frac{\partial}{\partial t}(\varepsilon_i \rho_i \boldsymbol{v}_i) + \nabla.(\varepsilon_i \rho_i v_i v_i) = -\nabla.\left(\boldsymbol{P}_{k,i} + \boldsymbol{P}_{c,i}\right) + \varepsilon_i \rho_i \boldsymbol{F}_i + N_{M,i}$$

Conservation equation for the fluctuating translational energy for species i:

$$\frac{9}{\pi d_i^3}\left[\frac{\partial}{\partial t}(\varepsilon_i \theta_i) + \nabla.(\varepsilon_i \theta_i \boldsymbol{v_i})\right] = \left(\boldsymbol{P}_{k,i} + \boldsymbol{P}_{c,i}\right) : \nabla \boldsymbol{v}_i - \nabla\left(\boldsymbol{q}_{k,i} + \boldsymbol{q}_{\boldsymbol{c},\boldsymbol{i}}\right) + \varepsilon_i \rho_i \langle \boldsymbol{F_i C_i}\rangle + N_{E,i}$$

3. Constitutive relations

Pressure tensor

$$\mathbf{P}_{k,\mathrm{ij}} = \frac{\rho_i \theta_i}{m_i}\mathbf{I} + \frac{4\mu_{s,dil}}{(1+e_{ij})g_o}\left(1 + \frac{4}{5}\varepsilon_{s,i} g_{ij}\left(1 + e_{ij}\right)\right)\nabla^s \mathbf{v}_i$$

Solid phase pressure

$$\boldsymbol{P}_{\mathrm{si}} = \frac{\rho_i \theta_i}{m_i} + \sum_j \frac{\pi}{48}\left(1 + e_{ij}\right) d_{ij}^3 g_{ij} \frac{m_i m_j n_i n_j}{m_o}\left(\frac{m_i m_j}{\theta_i \theta_j}\right)^{\frac{3}{2}} \frac{1}{A^{3/2} D^{5/2}}\left[1 + \frac{15\pi B^2}{4AD} + \cdots\cdots\cdots\cdots\right]$$

Solid shear viscosity

$$\mu_i = \sum_j \left\{ \frac{2\mu_{i,dil}}{(1+e_{ij})g_{ij}}\left(1 + \frac{4}{5}\varepsilon_{s,i} g_{ij}\left(1 + e_{ij}\right)\right)\left(1 + \frac{4\pi}{15} d_{ij}^3 n_j g_{ij} \frac{m_i}{m_o}\left(1 + e_{ij}\right)\right) + \frac{\sqrt{\pi}}{240\theta_i} g_{ij} d_{ij}^4 \left(\frac{m_i m_j}{m_o}\right)^2 \left(1 + e_{ij}\right) n_i n_j \left(\frac{m_i m_j}{\theta_i \theta_j}\right)^{3/2} S_1 \right\}$$

Dilute viscosity

$$\mu_{i,dil} = \frac{24\varepsilon_{si}\theta_i \rho_i}{\pi^2 d_i^3 m_i \sum_j N_{ij}}$$

Energy dissipation

$$\boldsymbol{N_{E,i}} = \sum_j \left(\gamma_{ij}^1 + \gamma_{ij}^2\right)$$

Reynolds-Averaged Navier-Stokes equations (RANS) were used in the study (please refer to Table 5). RANS equations are only mentioned in Table 5 and not elaborately presented here in this paper, as the use of RANS Equations is standard practice in CFD. The standard k-ε model was used in this study (Table 5). In the Standard k-ε model, the eddy viscosity is computed from turbulent kinetic energy and turbulent dissipation. This eddy viscosity is used in RANS Equations. The electrostatic forces between the particles were ignored in the present study.

In the present model, the transport equations were discretised using the finite volume method (FVM). To discretise the convective term, we employ a second-order upwind

scheme. This scheme is known for its ability to capture the directionality of flow and minimise numerical diffusion, especially in cases of high gradients. The diffusive term was discretised using a central differencing scheme, which provides second-order accuracy. This scheme is suitable for capturing diffusion effects accurately and maintaining stability. The source term was treated implicitly to ensure stability and accurate representation of the physics. We use the SIMPLE (Semi-Implicit Method for Pressure-Linked Equations) algorithm to handle the pressure-velocity coupling and ensure the pressure-velocity decoupling is carried out efficiently.

3. The CFB System

The CFB system experimentally investigated at Telemark Institute of Technology is shown in Figure 1. The riser was cylindrical in shape with an internal diameter of 0.032 m and a height of 1.0 m. The primary gas inlet was located at the bottom of the riser. In order to provide a uniform gas velocity at the inlet, an air distributor was installed. The distributor was a Duran filter plate with a thickness and porosity of 0.004 m and 0.36, respectively. At the top of the riser, the suspended particles enter a glass cyclone where the solids are separated from the gas and recycled via a return loop. Supply of secondary air positioned at 0.05 m above the air distributor feeds the solids back to the riser. Figure 1 shows a schematic sketch of the circulating fluidised bed system used in the experiment.

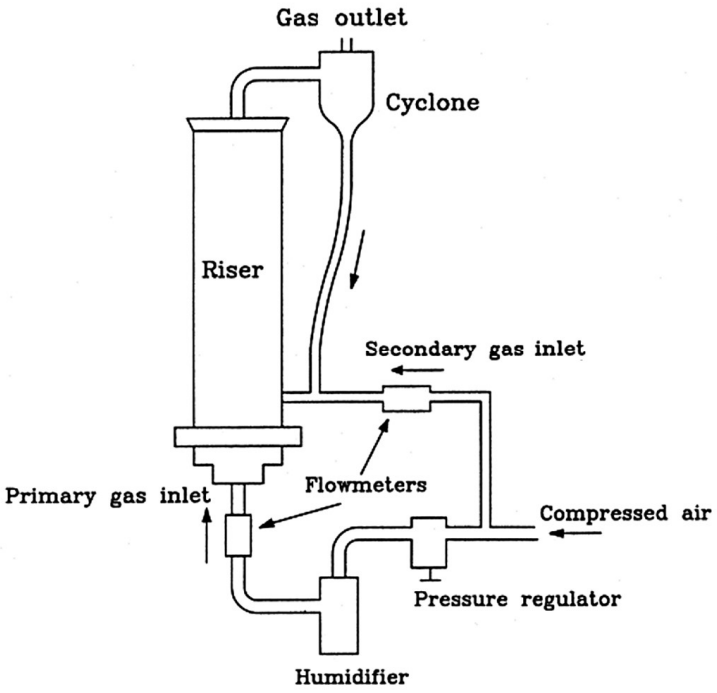

Figure 1. A schematic sketch of the laboratory scale CFB Mathiesen [30].

Two distinct particle groups were sieved out from a Gaussian particle size distribution with a Sauter mean diameter of 157 μm. The diameters of the sieved particles are between 100 and 130 μm and between 175 and 205 μm for the smallest and largest particles, respectively. The mean particle diameters of the two groups were approximately 120 and 185 μm. The two distinct groups were mixed together, and the initial volume concentration of each group was identical. The particle density was 2400 kg/m^3. The initial bed height was 0.04 m. Thus, the overall volume concentration of solids in the riser is 2.5%. The flow parameters used in this work have been shown in Table 2.

Table 2. Numerical flow parameters used in this work.

Riser Dimensions-Cylindrical	Diameter	0.032 m
	Height	1.0 m
Operating conditions	Gas phase	ρ_g = 1.2 kg m^{-3}, μ_g = 0.00001 Pa s
	Solid Phase I	ρ_{sI} = 2400 kg m^{-3}, d_I = 120 μ_m
	Solid Phase II	ρ_{sII} = 2400 kg m^{-3}, d_{II} = 185 μ_m
	Initial bed height	0.04 m
	Pressure	Atmospheric pressure
	Inlet gas velocity	J_g = 1.2 m s^{-1}
	Fraction of solids	0.63

4. Grid and Physical Domain

Only the riser part of the circulating fluidised bed shown in Figure 1 has been modelled. In order to avoid convergence difficulties, the calculation domain is divided into five blocks. The grid characteristics and the grid information are listed in Tables 3 and 4.

Table 3. Grids statistics.

Property	Minimum	Maximum	Average
Volume	1.878×10^{-8}	5.565×10^{-8}	3.499×10^{-8}
Skew	0.9	1.0	0.9752
Twist	1.0	1.0	1.0
Taper	0.7588	1.0	0.8597
Stretch	0.6362	1.0	0.8585

Table 4. Grids information.

Block	NI	NJ	NK	NCell
1	6	4	200	4800
2	6	4	200	4800
3	6	4	200	4800
4	4	4	200	3200
5	6	4	200	4800
Total number of grid cells				22,400

The grid independence test was performed for this study through the simulation of gas flow in the riser. Starting with a lower number of cells of 5600 in the riser, the number of cells in the riser was extended up to 33,600 in four steps. The calculated results for each step have been shown in Figure 3. It has been observed from Figure 3 that with the increase in cell number beyond 22,400, the velocity is independent of the number of cells. Therefore, for this study of the riser flow CFB, 22,400 cells have been used for further simulations. In this test, mass source residual (error in continuity) is used to control the convergence of the solution, and the tolerance limit was set to 10−6. In this simulation, the equation for continuity, momentum and transport equation for k and ε were solved for turbulence parameters.

5. Boundary and Initial Conditions

In this work, a wall boundary, inlet and outlet boundaries are used. The inlet boundaries are given by a specific inflow velocity and volume fraction. The inlet velocity and volume fraction used in this simulation are given in Table 2. At the outlet, a pressure boundary condition with atmospheric pressure has been used. This essentially applies constant gradient conditions to the flow variables. Solids are also permitted to leave through the boundary. Buoyant flow has been enabled with gravity of 9.81 m/s^2.

For a gas, the no-slip wall condition is well accepted and used. However, for walls that are both non-slip [17,33] and free-slip [34], solid velocity conditions have been used by different researchers. In general, it is not permissible to set the particle velocity equal to zero at a solid wall. Exceptions occur when the wall is sufficiently rough, minimising particle slip and when the bounding wall is sufficiently soft, creating highly inelastic particle–wall collisions. Tsuo and Gidaspow [35] used a partial-slip boundary condition, which is between the two mentioned conditions. Insufficient numerical and experimental work has been undertaken to show any boundary condition as being superior with all capable of predicting clusters. In non-slip boundary conditions near the wall, some fluid (for example, a layer of fluid molecule/molecules) is assumed to attach to the solid wall, whereas in no slip boundary condition, fluid does not attach to the solid wall. Slip boundary conditions are used to model the behaviour of particles near solid surfaces, where the particles experience a slip velocity relative to the fluid due to a lack of adhesion. The choice of slip condition can indeed influence the results of simulations, and using different slip models, such as partial slip conditions or incorporating slip lengths, could provide valuable insights into the role of slip in the observed deviations. In our study, we chose a slip boundary condition based on the available literature and its relevance to the specific system we were simulating.

In this work, the riser is initially filled with a 0.04 m high bed where the total volume fraction of solids is approximately 0.63. The initial volume fractions for each individual phase have been show in Figure 2. The two solid phases are perfectly mixed in the bed and are assumed to have an identical initial volume fraction. In order to avoid convergence difficulties, the initial volume fraction of the solids above the bed in the computational domain is set to 1.0×10^{-10}, and to ensure a small initial viscosity, the granular temperature has been set to 1.0×10^{-10} in this work.

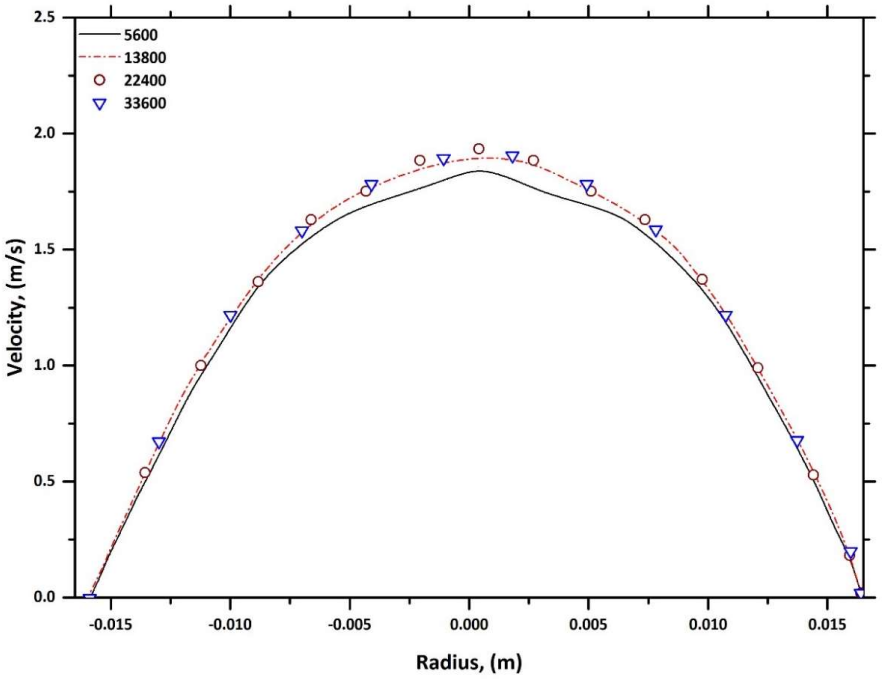

Figure 2. Grid independence test.

The proposed multi-particle kinetic theory of [3,21,31] was implemented in the commercial CFD code CFX through user subroutines. A time step of 0.001 s is used for the calculations. The under-relaxation factor used for the velocities and volume fraction was 0.3, and for the granular temperature, it was 0.2. Typically, 32.5 h of computational time is required on an Intel Pentium 4 (Xeon) 2.0 GHz computer to simulate one second of real-time. A summary of the model formulation used in the present work is introduced in Table 5.

Table 5. Summary of the model formulation.

Commercial Software	**CFX**	
General	Linear solver type	GSTB
	Pressure formulation	SIMPLE
	Run mode	Unsteady, $\Delta t = 0.001$ s
	Total time	32.5 h
	Gravitational body force	Full body force–Y direction
	Convergence criteria	0.0001
	Mesh type	22,400 grids, symmetric grid
Models	The Eulerian–Eulerian flow approach using Reynold's Averaged Navier Stocks (RANS) and continuity Equations	
	Drag model	Schiller–Neumann Equation for particles [36].
	Turbulence model	Viscous-standard k–ε, dispersed
Control	Number of phases = 2	
	Continuous phase = solid	
	Secondary phase = gas	
	Minimum volume fraction	1×10^{-6}
Boundary conditions	Inlet condition	Normal velocity, 10% mean kinetic energy for k.
	Outlet condition	Static pressure, 100,000 Pa, zero gradient for k-ε.
	Wall condition	No slip conditions

6. Results and Discussion

6.1. Solid Velocity Profile

Figure 4 shows the instantaneous velocity vectors at 21.0 s for the gas and the solid phases. The solid phase with smaller diameter (120 µm) particles is classified as Solid1, and the solid phase with a larger diameter (185 µm) has been classified as Solid2. A subsection of the physical domain has been enlarged in order to illustrate the flow pattern. A close-up view of the velocity vectors for gas, Solid1 and Solid2, are shown in Figure 3, respectively.

In studying Figure 4, it has been observed that the flow pattern for both solid phases is a core–annulus type of flow. A similar trend was found by [24,35,37]. Near the centre of the riser, there is an upward, rapidly moving core surrounded by a downward, relatively slower-moving annulus near the wall. The flow was started with a packed bed of solids at the bottom of the riser. Initially, the solids and the gas moved uniformly in a plug flow mode. Skin friction for air at the wall modified the flow by reducing the velocity in the near-wall region. The imposed velocity gradient caused by the wall pushed the particles towards the wall in the radial direction. This caused cluster formation, and particles started accumulating in the form of clusters in the near wall region. The cluster behaves as a hydrodynamic unit or as a particle of large effective diameter. Hence, the gravitational force acting on the cluster becomes higher compared to the drag force, and particles start to move downwards. Figure 4 shows these negative velocities of the clusters. Thus, an

annular region formed near the wall. In order to conserve the inlet constant mass flow, the upward velocities for both the gas and the solid phases in the core region had to increase in order to compensate for the additional area occupied by the downward-flowing annular region. Eventually, the upward and downward flow reaches a quasi-equilibrium state.

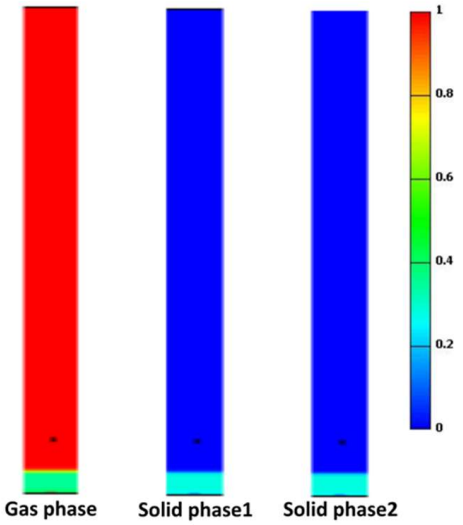

Figure 3. Initial volume fractions in the riser of the simulated CFB.

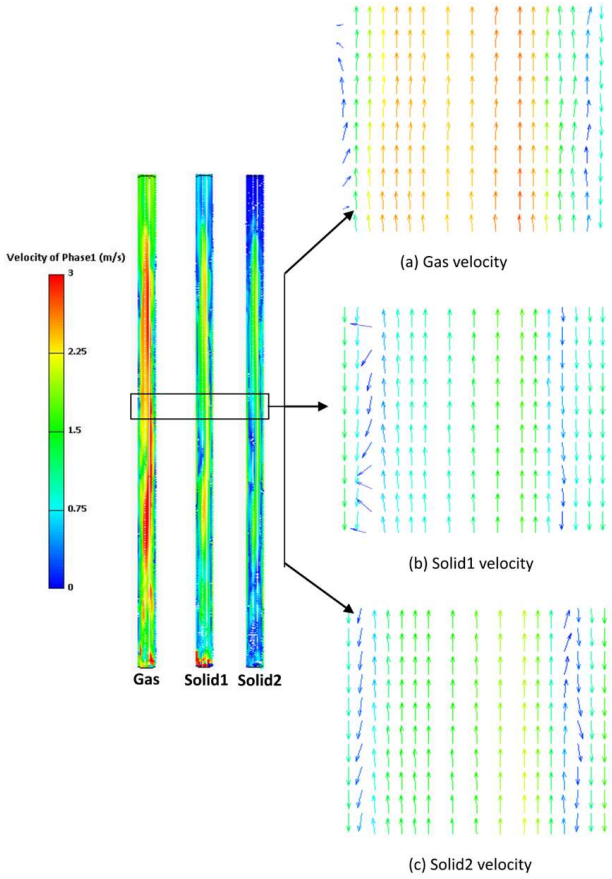

Figure 4. Instantaneous velocity vectors in the riser at t = 21.0 s.

From Figure 4, it can be observed that the velocity on the right side of the core is higher as compared to the velocity on the left side of the core for both gas and solid velocities. As

Figure 4 illustrates, with the instantaneous velocities, some local variations are expected due to the influence of transient void distribution in the riser. However, when the mean velocities for the gas as well as the solids were plotted, the ideal core–annular flow can be observed, as shown in Figure 4. This core annular flow pattern shows that all three phases are moving upward through the central region. However, the velocity of the gas is higher than that of the solid phases. It should also be noted that the Solid1 particles move faster than the Solid2 particles. Figure 5 also clearly shows that particles are falling down under gravity along the wall, whilst in the centre of the riser, a core of upward-moving gas and diluted solids has been formed. Particles with a smaller diameter (Solid1) travel at higher velocities when compared to the particles with a larger diameter (Solid2) in both core and annular regions. This is due to the smaller gas–particle drag force required to accelerate the particles of smaller diameter. A similar trend was found in Mathiesen and Solberg's [20] experimental data under identical conditions. It has been observed from Figure 6 that with the increase in height, the width of the core region increases, which is consistent with observations of [38].

(a).

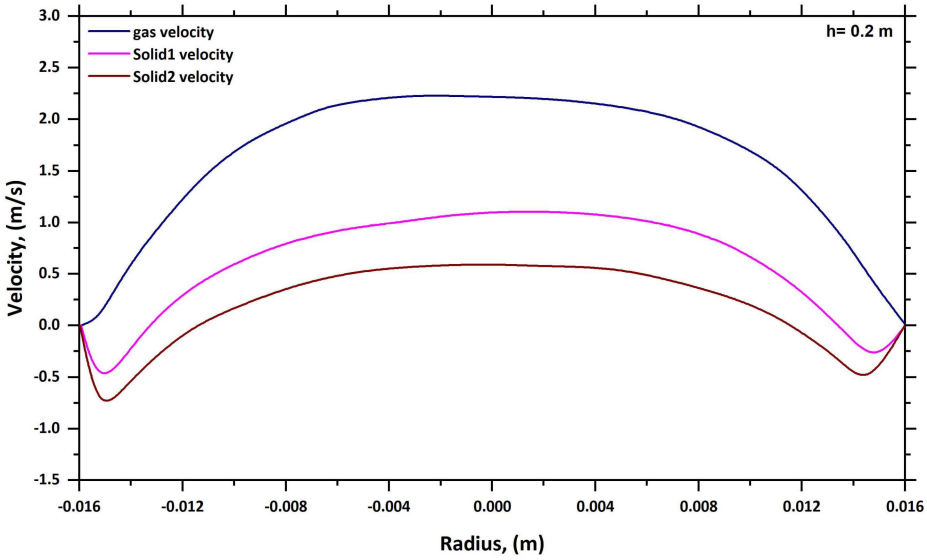

(b).

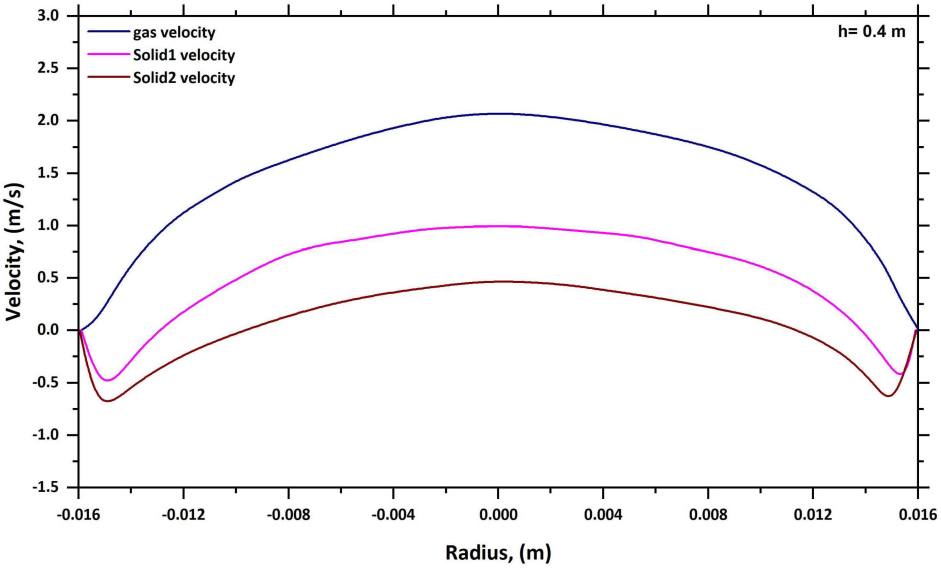

Figure 5. *Cont.*

(c).

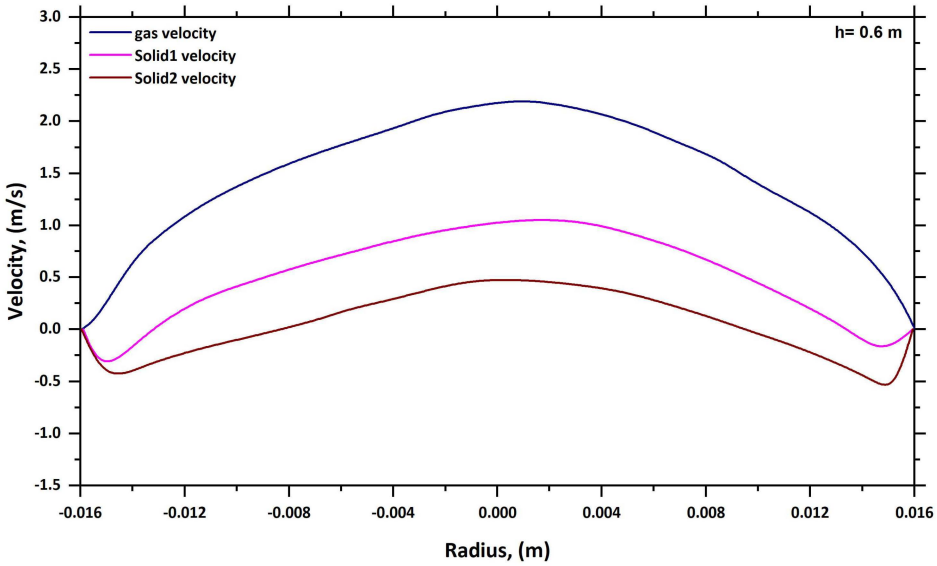

Figure 5. Velocity profiles at different height of the riser; (**a**) h = 0.2 m, (**b**) h = 0.4 m and (**c**) h = 0.6. m.

(a).

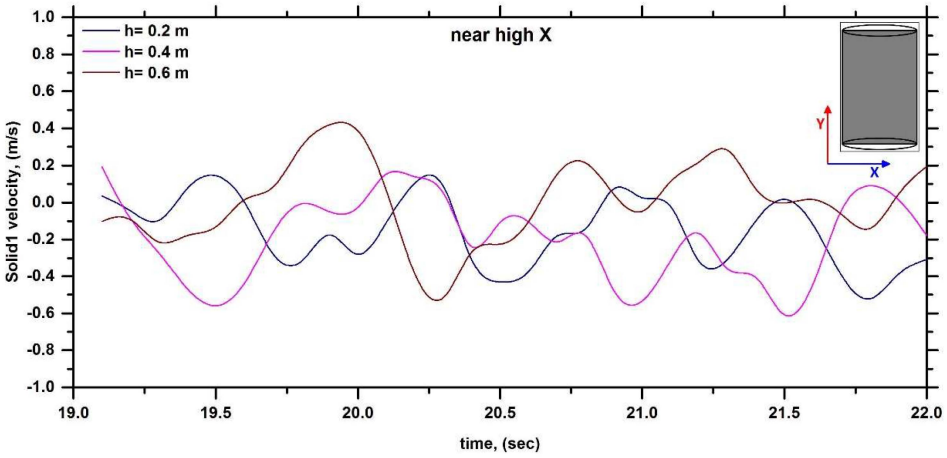

(b).

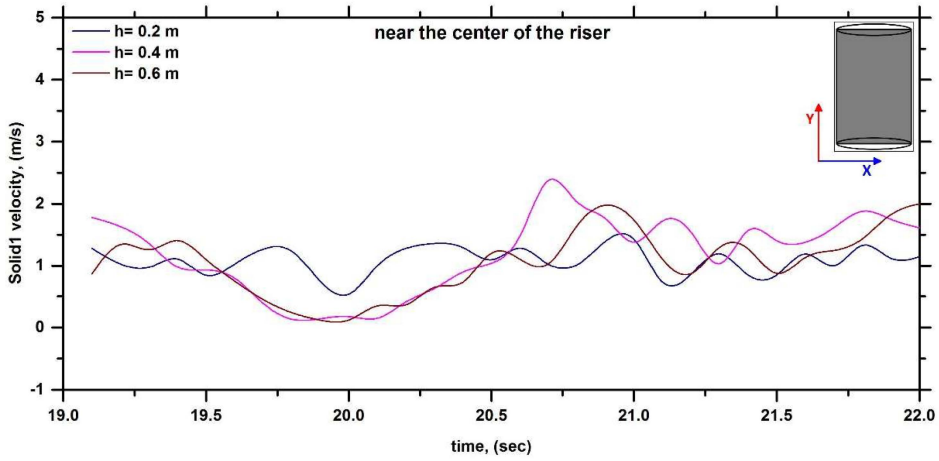

Figure 6. *Cont.*

(c).

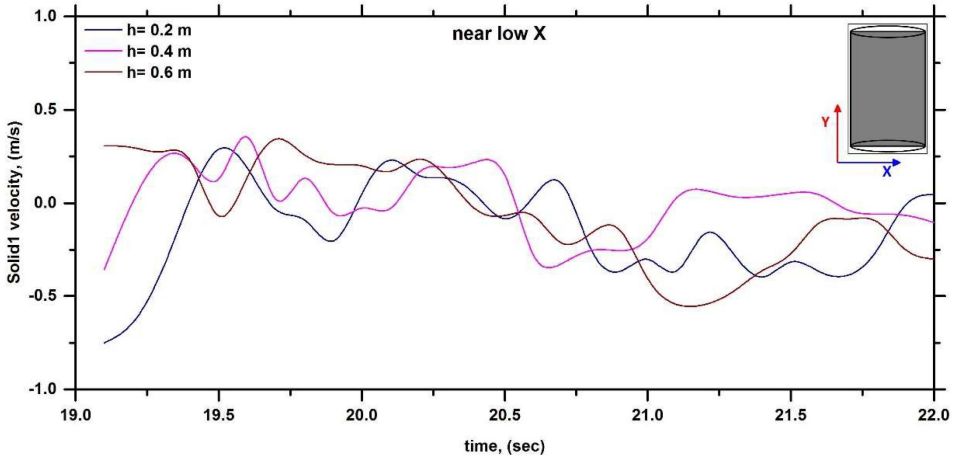

Figure 6. Influence of height on Solid1 velocity variation with time; (**a**) near high X, (**b**) near the centre of the riser and (**c**) near low X.

Figures 6 and 7 show the transient velocity variation in the solids with time at different heights, low x, centre and high x of the riser. Results presented in these figures show a similar behaviour near both walls with substantial fluctuations present in both solid phases. The Solid1 velocity predicted near the riser walls (low and high x) oscillates between an upward velocity of 0.3 m/s and a downward velocity of 0.6 m/s. However, in the centre, the solid velocity oscillation is higher compared to the oscillations near the wall. Near the centre, the Solid1 particle velocity fluctuates between 0 m/s and 3 m/s in an upward direction. The Solid2 velocity predicted near the riser walls (low and high x) oscillates between an upward velocity of 0.1 m/s and a downward velocity of 0.7 m/s. Near the centre, the Solid2 particle velocity fluctuates between 0 m/s and 2.5 m/s. Significant oscillations of the velocities with time were observed in Figures 6 and 7. As Figures 6 and 7 illustrate for the instantaneous velocities, some local variations are expected due to the transient nature of the system, resulting in velocity fluctuations. Similar trends were found in single-phase fluidised bed models by [16,33]. For multi-particle flow, measurements of the velocity variation with time along the wall region are not available in the literature, making validation of these predictions of wall velocity difficult. Figures 6 and 7 confirm a stochastic flow behaviour in the riser. The particle's velocity is almost always negative, close to the wall. In the central part of the riser, the oscillating velocity includes negative and positive values, but a much higher fraction of the particles is flowing upward than downward.

(a).

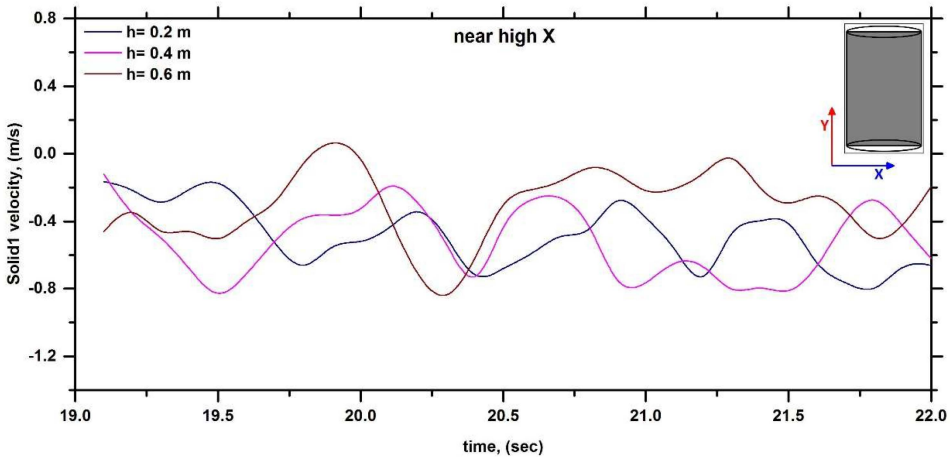

Figure 7. *Cont.*

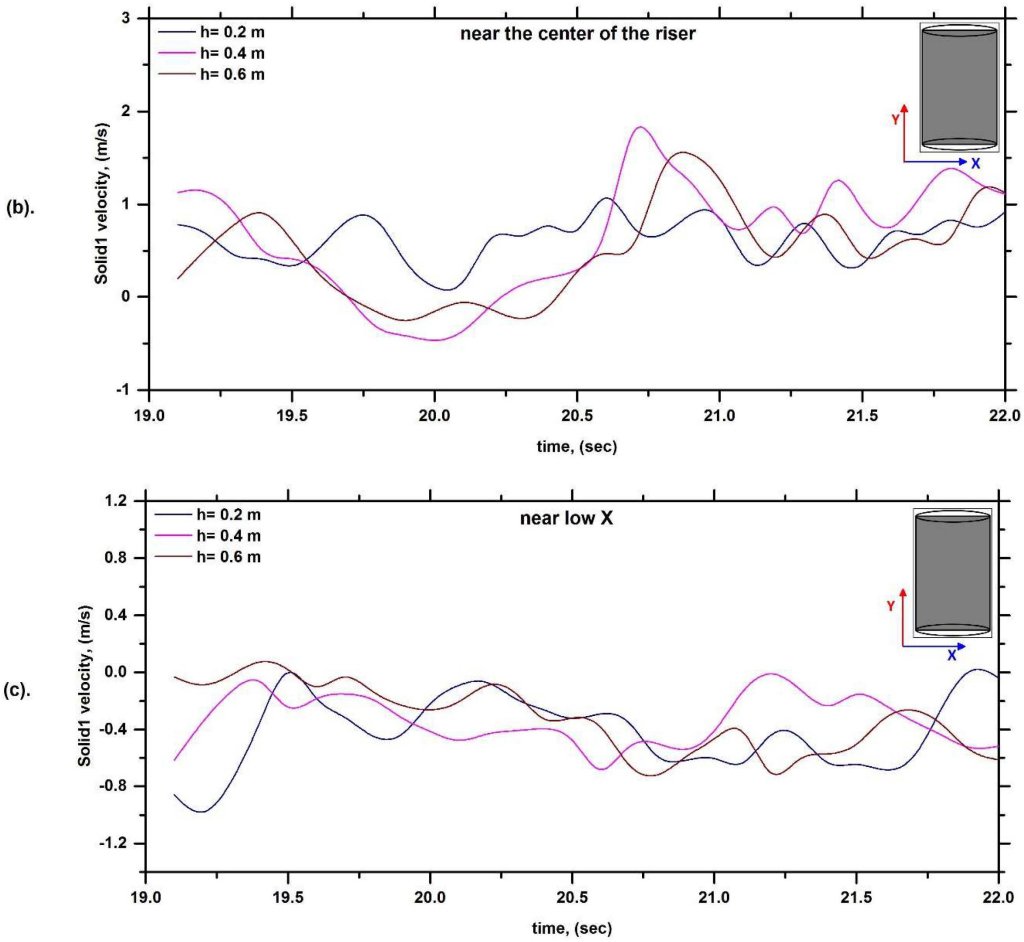

Figure 7. Influence of height on Solid2 velocity variation with time; (**a**) near high X, (**b**) near the centre of the riser and (**c**) near low X.

6.2. Validation of the Numerical Results

Figure 8 shows the measured and computed particle velocity profiles for both solids (Solid1 and Solid2). The particle velocity profiles are obtained with a superficial gas velocity of 1.0 m/s and are at a height of 0.4 m above the gas inlet. As discussed earlier (Section 6.1), core–annulus flow is predicted in the riser. The behaviour is clearly observed in the simulation as well as the experimental work of [20,30]. The measured velocity profiles show a relative velocity between the two solid phases in the core region. In the wall region, no significant relative velocity was observed on the left side of the experimental velocity profile, and significant relative velocity was observed on the right side of the experimental velocity profile. However, the computed results indicate a significant relative velocity between the solids in the core region as well as in the wall region. The relative velocity is expected in the core region as well as in the wall region. The relative velocities are caused by different values of gas–particle drag for the different-sized particles. The particle–particle drag, which is a function of the particle–particle collisions, will also play a major role in determining the magnitude of the relative velocity.

Though the proposed model correctly predicted the velocity trend in the core region, it can be observed that it has over-predicted the downward velocities of the solids in the near-wall region. This over-prediction of the downflow velocities may be due to the fact that electrostatic forces were present in the experiments and were not incorporated into the model. As mentioned earlier, Miller and Gidaspow [38] reported the presence of much static electricity in the CFB system. Their observation shows that the particles were attracted and almost glued to the wall were observed. Another cause may be in the selection of wall boundary conditions. In this work, the free slip boundary condition was used for the solid

phases. The use of partial slip boundary conditions might provide a better prediction in the wall region. In the core region, this model correctly captures the trend of the velocity. The magnitudes of the velocities are in reasonably good agreement with the experimental results. It has been observed that the model over-predicts the velocity of Solid1. However, the predicted velocity of Solid2 is in good agreement with the experimental results. This may be attributed to the gas–particle drag model used in this study.

The results of Mathiesen [30] for particles of different sizes are reproduced in Figure 9. A comparison of Figures 8 and 9 shows that the proposed model can capture the trend of the velocities more preciously than Mathiesen's model in the core region. However, in the annular region, the Mathiesen [30] model provides a better prediction compared to the proposed model. This is due to the wall boundary condition used in the model, as discussed in Table 5. In this model, a slip boundary condition was used. However, in Mathiesen's model, a no-slip boundary condition was used. The use of partial slip boundary conditions might provide a better prediction in the annular region. It has been observed from Figures 8 and 9 that both models predict higher relative velocities between the solids compared to the experimental prediction. The reason behind this might be the gas–particle drag model, as mentioned earlier in this section. Another reason may be the uncertainty of the mean diameter of the particle size distribution reported by Mathiesen [30]. A small error in the mean diameter may give rise to a significant rise in the drag terms, causing the over-prediction of the velocities. Since no other experimental data for a gas–solid flow system with different-sized particles are available in the literature, a more detailed validation of the proposed kinetic model is not possible at this stage. Though some variations in the magnitude of the solid velocities are observed compared to the experimental results, the proposed model predicted the trend of the velocity profile more accurately than the earlier models. To obtain better validation of the model requires better quality experimental data for a system with two single particle sizes and greater details of solid volume fraction, pressure drops and gas velocity.

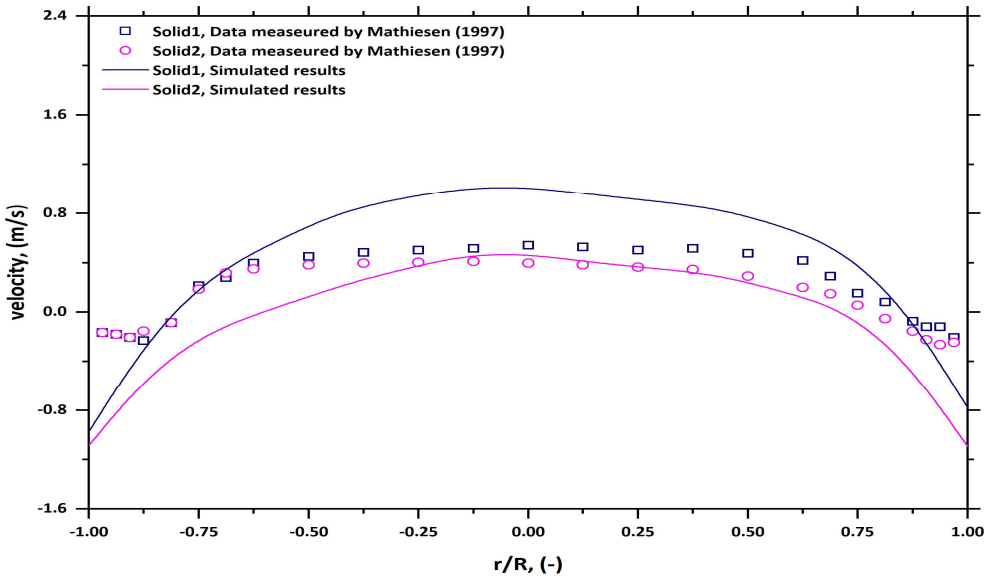

Figure 8. Simulated particle velocity profiles with proposed kinetic theory model [30].

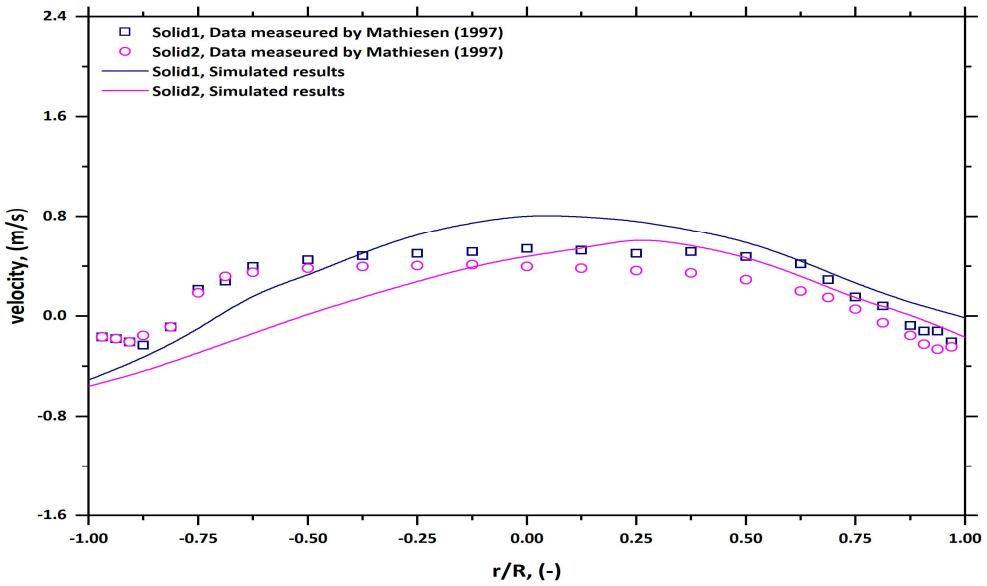

Figure 9. Simulated particle velocity profiles with previous kinetic theory model [30].

6.3. Volume Fraction Profile

Figure 10 shows the computed radial time-averaged volume fraction profiles of solids at different riser heights. Time-averaging was performed over the last two seconds of the 21 s of the real-time simulation. This was selected in order to isolate a period of relative stability and relevance to the observed system's behaviour. This approach enhances the accuracy of the comparison with experimental data and provides a clearer understanding of how well the model aligns with real-world dynamics. At all locations, the solid volume fraction distribution shows the expected trend, a dilute region in the core and denser flow near the wall. As expected, the solid concentration is highest near the base of the riser at 0.05 m and decreases with the increase in height. Since no experimental data for volume fraction are available, no comparison with the experimental results can be shown. The simulated volume fraction profile shows the trend of core–annular flow. Similar trends were observed in other numerical and experimental model results [33,38] for mono-particle flow in a CFB riser. At 0.05 m height, the solid volume fraction at the right riser wall is predicted to be higher than that at the left riser wall. The reason for this occurrence has been explained later on in this section.

Figures 11 and 12 show the computed volume fraction distribution at different time intervals between 20 and 21 s for Solid1 and Solid2. In Figure 11, a cluster and gas void formation can be observed at different time intervals for Solid1. At 20.1 s, the formation of the gas void is observed near the bottom of the riser. With the increase in time, the formatted void expands up the riser, with the gas gradually tunnelling through the solids. This gas–solid interaction causes the solid material to separate towards the walls, resulting in a lower concentration of solids close to the centre of the riser and an increase in solid concentrations towards the walls. In the region close to the wall, cluster formation can be observed, and the solid particles move downward under gravitational force. Hence, a circulation of solids can be observed in the riser with a strong upward flow of the solid at the centre, gradual migration of solids towards the wall and a downward flow of solids in the near wall region. Figure 12 illustrates the Solid2 volume fraction in the lower section of the riser. It can be observed from Figure 12 that most of the solids remain at the bottom of the riser in the form of a turbulent bed, indicating particle separation.

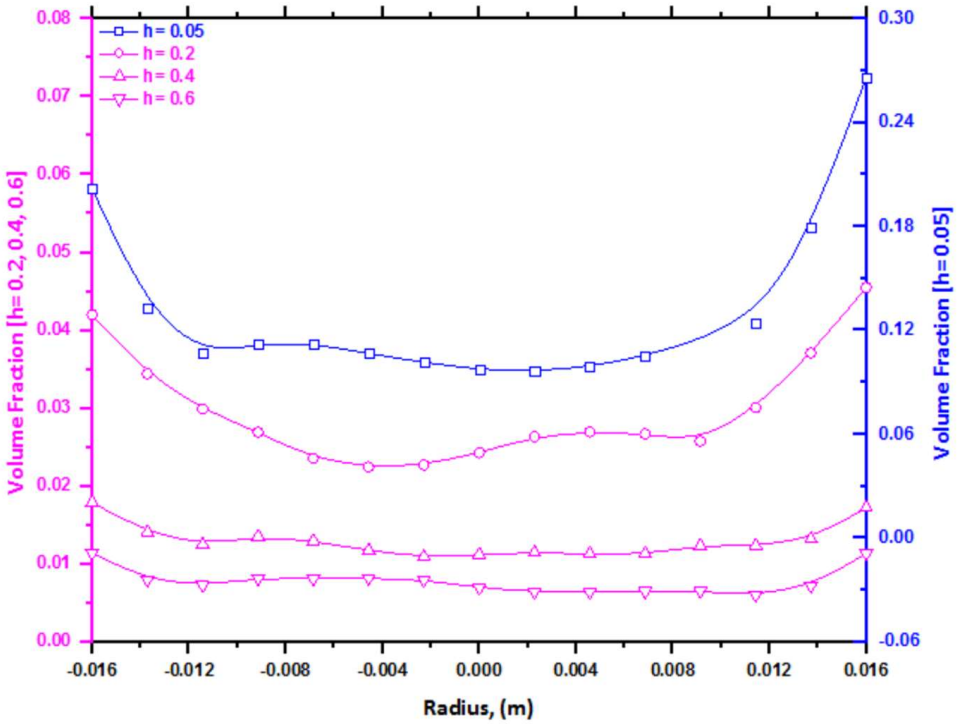

Figure 10. Time-averaged solid volume fraction at different heights.

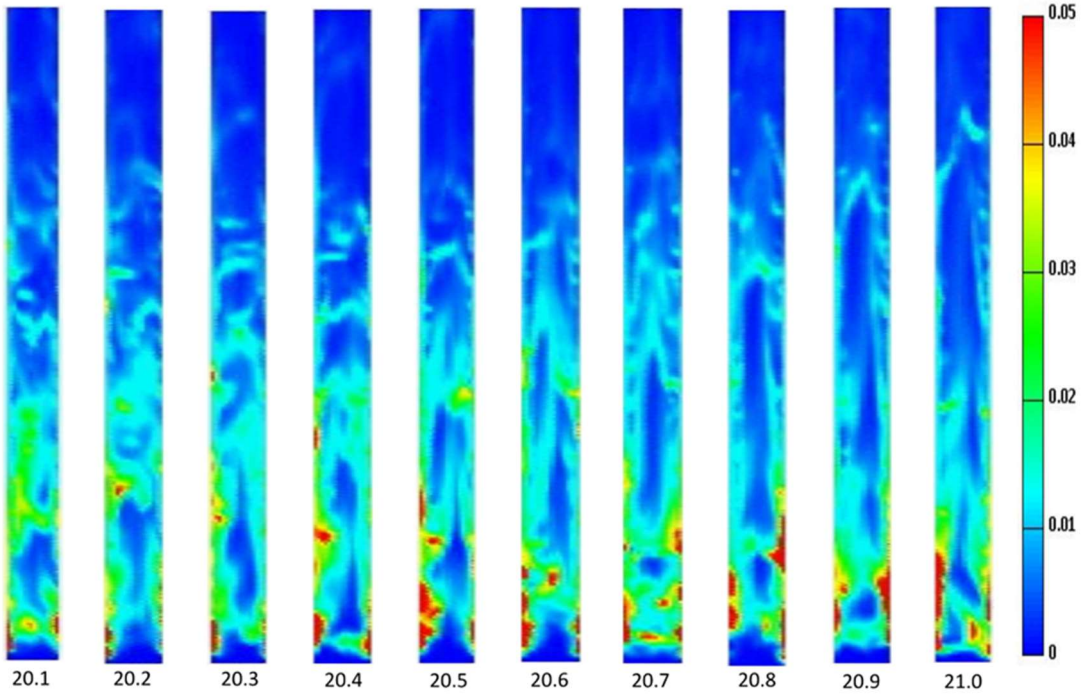

Figure 11. Solid1 volume fraction distribution in the riser (time = 20.1–21.0 s).

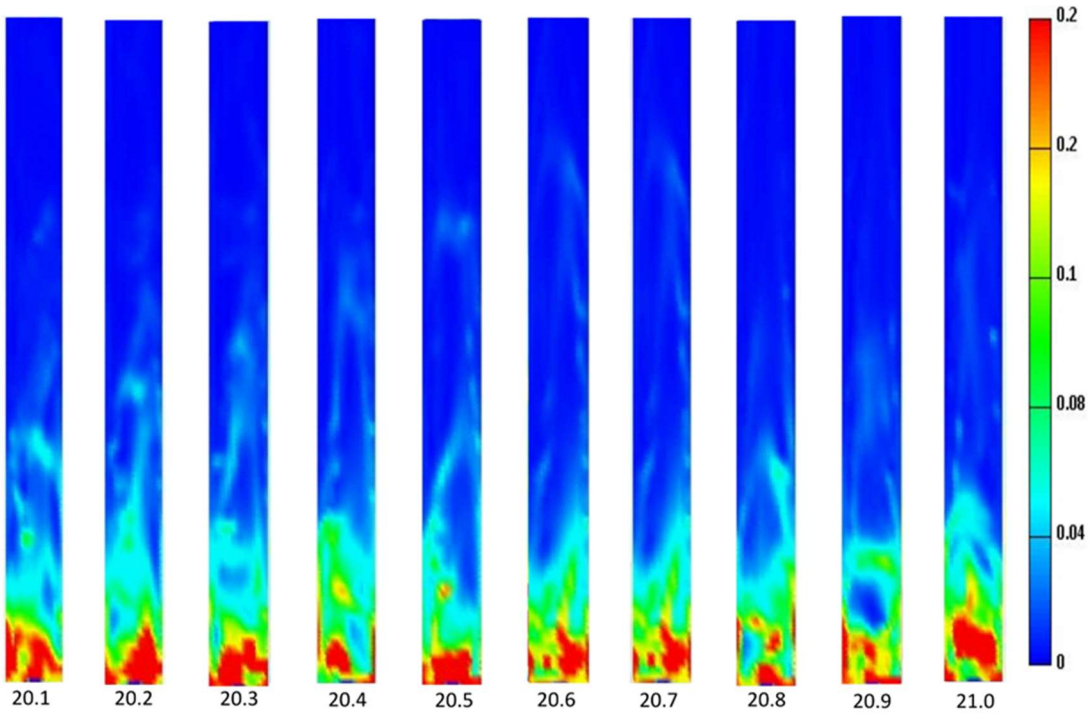

Figure 12. Solid2 volume fraction distribution in the riser (time = 20.1–21.0 s).

The mention of particles being recirculated downwards in the lower half of the riser indicates that there's a tendency for particles to move downwards instead of uniformly rising. This phenomenon can be attributed to the complex interplay of various hydrodynamic forces and particle interactions in the riser. The interaction between these forces and the particles themselves contributes to the observed behaviour. For instance, particles might collide and clump together due to these forces, causing them to become denser and heavier. As a result, these denser clusters tend to settle in the lower portion of the riser, counteracting the upward flow. This interplay of forces and particle behaviours leads to a non-uniform distribution of particles, ultimately causing the widening of the core region with an increase in height. Understanding this intricate relationship between hydrodynamics and particle interactions is crucial to comprehending the complex behaviours observed in the system.

Figures 13 and 14 show the transient fluctuation in the solid's volume fraction at different heights and at the riser centre line, low x and high x. It has been observed from the figures that with the increase in height, the solid volume fraction fluctuation decreases, which is expected as solid velocity reduces with the increase in height. By studying Figure 13, it can be observed that at 0.2 m height, near the centre of the riser, the Solid1 concentration fluctuates more compared to that at 0.4 m and 0.6 m height. In near-wall regions (low and high x), the solids fall down under gravity and return to the bottom of the riser. At the bottom, the returned solids move upward with incoming gas in the form of clusters. With height, the solid materials separate towards the wall as the gas gradually tunnelling through the solids. Therefore, in the lower section of the riser, 0.2 m, more cluster formation can be observed and hence, higher fluctuations in the solid volume fraction are expected when compared to that in the upper section of the riser. Figure 14 illustrates the Solid2 volume fraction in near-wall regions (low and high x) as well as close to the centre region. In Figure 14, a similar trend to that of the Solid1 volume fraction (Figure 14) can be observed for the Solid2 volume fraction. However, the Solid2 volume fraction at the upper portion of the riser is very low due to the greater particle diameter and, thus, has a higher terminal velocity.

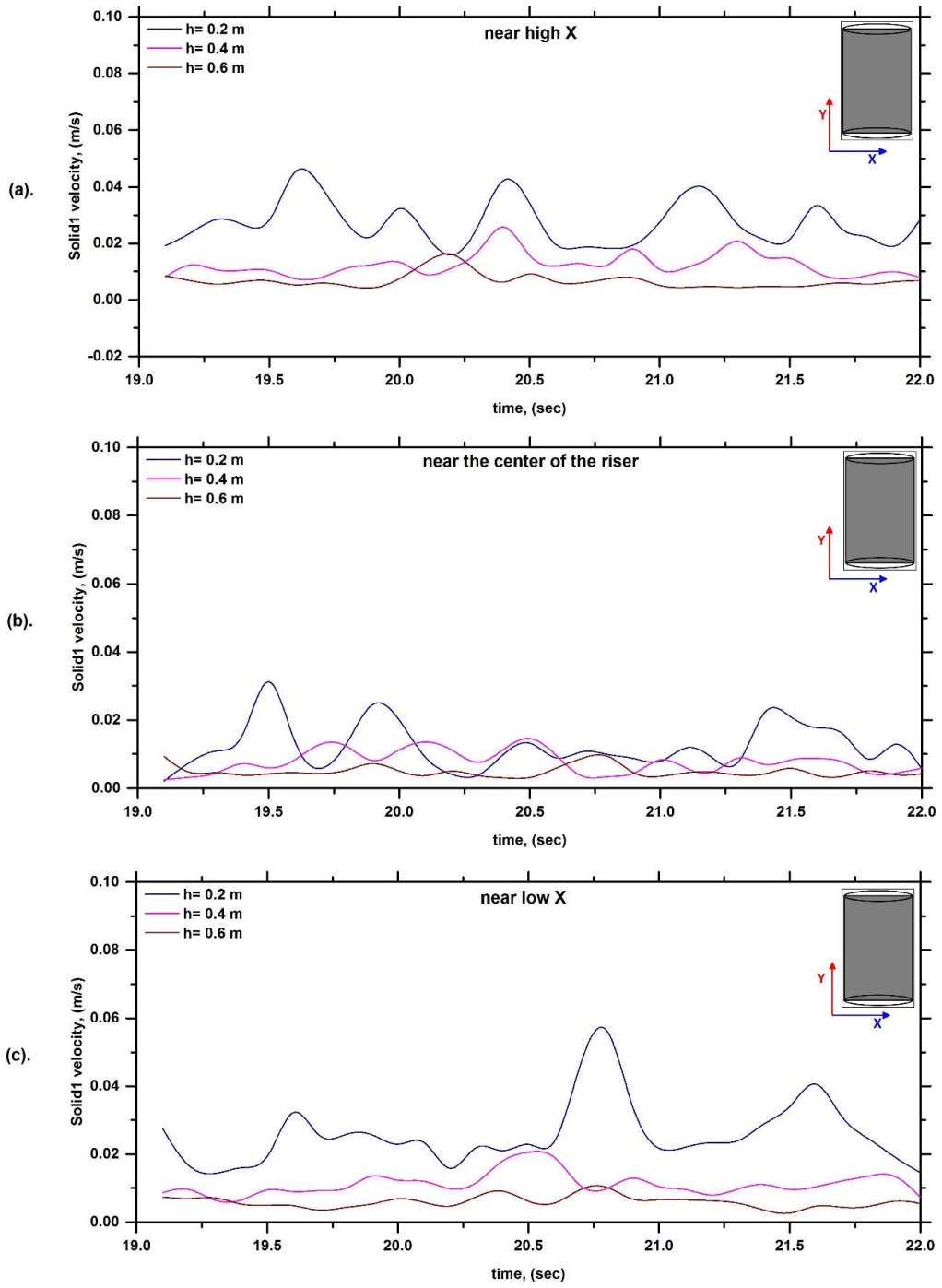

Figure 13. Influence of height on Solid1 volume fraction variation with time; (**a**) near high X, (**b**) near the centre of the riser and (**c**) near low X.

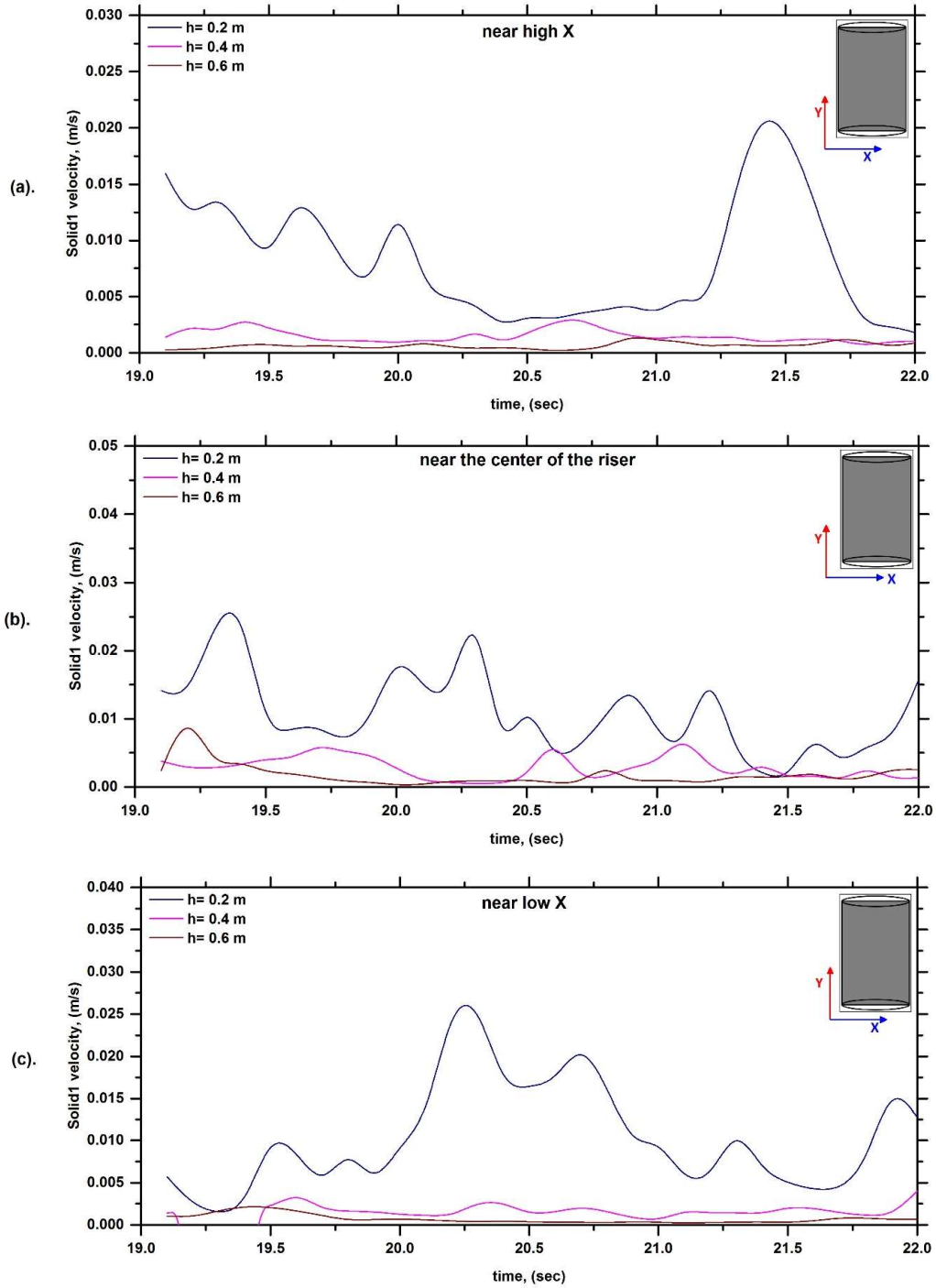

Figure 14. Influence of height on Solid2 volume fraction variation with time; (**a**) near high X, (**b**) near the centre of the riser and (**c**) near low X.

6.4. Granular Temperature Profile

Figure 15 shows the time-averaged granular temperature distribution for both solid phases at different heights. It can be observed from Figure 15 that the granular temperature for lighter particles (Solid1) is reasonably uniform in the core region. In the annular region, the magnitude of the granular temperature decreases towards the walls. This is expected as, in the wall region, the concentration of the particles increases (See Figure 11), resulting in less room for the particles to oscillate. Since the solid concentration is low in the core region, the particles have more space to fluctuate, resulting in high fluctuations, thus leading to a high granular temperature. It can be observed from Figure 15 that no drastic change

in granular temperature is found in the transition region between the annular and core. However, in the transitional region, the velocity gradient is high (as the solids are moving downward in the core region and upward in the annular region), which should increase the magnitude of the shear stress and energy dissipation and, hence, granular temperature. Since the diameters of the particles are very small, the change in the magnitude of shear stress and energy dissipation due to the velocity gradient is insignificant. Therefore, no significant difference in the granular temperature between the near wall and core region was observed in the predicted results. For heavier particles (Solid2), there is no significant variation in granular temperature in the core and annular region. It can be observed from Figure 12 that the particles of Solid2 remain at the bottom of the bed due to the lower gas velocity compared to that required to transport them up the riser. Thus, at a height of 0.2 m, the volume fraction of Solid2 is very small, resulting in an almost constant fluctuation of velocity and, hence, a constant granular temperature.

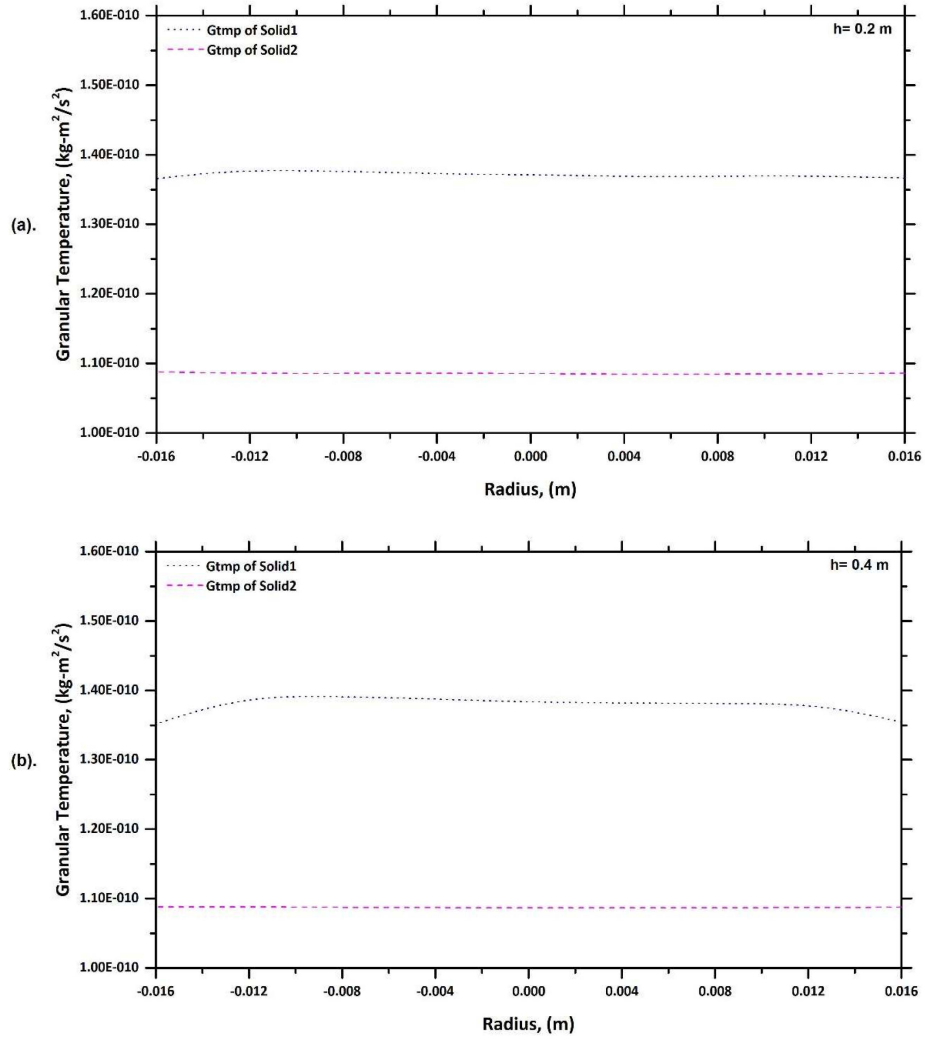

Figure 15. *Cont.*

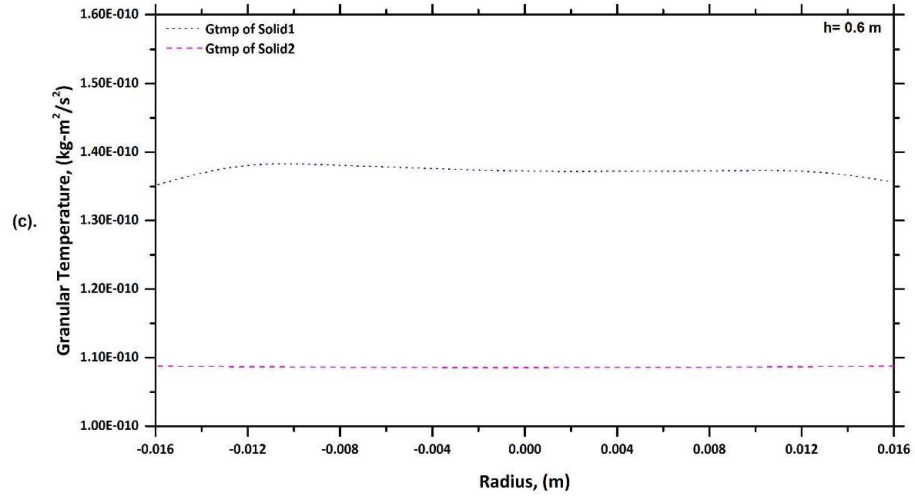

Figure 15. Time-average granular temperature profile at different heights of the riser; (**a**) h = 0.2 m, (**b**) h = 0.4 m and (**c**) h = 0.6. m.

Differences in the granular temperature between the two solid phases can be observed at all heights in the predicted results. Previously, Farrell and Lun [39] have speculated that the assumption of an equal granular temperature for the two phases might not be realistic, and Jenkins and Mancini [40] suggested that different granular temperatures be used for particles with different masses. In the current model, this concept of different granular temperatures has been used, and a variation in granular temperature between the solid phases (Figure 15) was predicted. With the above discussion and results it can be concluded that models with unequal granular temperature can be used to obtain improved results of the flow behaviour in a gas–solid flow system with different-sized particles.

7. Conclusions

In this work, a new kinetic theory (KT) model for particles of different densities and sizes has been implemented in the commercial CFD software CFX and used to simulate the riser section of a circulating fluidised bed having particles of different sizes. Different flow properties for solid phases, such as solid viscosity, solid pressure, collisional heat flux and bulk viscosity resulting from particle–particle interactions, are obtained from the present CFD model. Interphase transfer terms (i.e., momentum transfer and fluctuating energy transfer) between the solid phases are also implemented into the CFD model through user-defined functions (UDFs). The k-ε turbulence model is used in simulating the circulating fluidised bed model. For verification, simulation results obtained with the new KT model are compared with experimental data, and then the model is used for further analysis. Using the CFD model, results were obtained for a three-dimensional circulating fluidised bed model that are in fairly good agreement with experimental results. The model successfully predicts typical CFB behaviour, such as

- Core–annular flow in the riser,
- Particle carryover,
- Cluster formation,
- Downward particle flow near the riser wall,
- Relative velocity between particles of different sizes,
- Different granular temperatures for particles of different sizes,
- A turbulent bed of large diameter particles in the base of the riser and transport of the smaller particles well in the top section of the riser,
- A higher concentration of solids in the wall region compared to the centre.

The predicted results are in qualitative agreement with published experimental work. This indicates that the multi-particle multiphase gas–solid flow model works fairly well.

Author Contributions: Methodology, F.R., A.A.R.S. and J.N.; Validation, F.R.; Writing—original draft, F.R.; Writing—review & editing, A.A.R.S.; Visualization, A.A.R.S.; Supervision, J.N. All authors have read and agreed to the published version of the manuscript.

Funding: This research received no external funding.

Data Availability Statement: The data supporting the findings of this study is available upon request.

Conflicts of Interest: The authors declare no conflict of interest.

Nomenclature

A	Particle projected area
C_d	Drag coefficient
C_g	Fluctuating velocity of gas
c_i	Instantaneous velocity of particle i
c_{ij}	Relative velocity
c_j	Instantaneous velocity of particle j
C_p	Fluctuating velocity of particles
d	Diameter of particle
D_w	West diffusion coefficient
e	Restitution coefficient
F	Total external force
f_i	Velocity distribution of phase i
f_j	Velocity distribution of phase j
F_p	Particle drag force
G	Combined velocity during collision
g	Radial distributive function
h_w	Distance between west and central nodes
I	Unit tensor
m_i	mass of particle i
m_j	mass of particle j
m_k	mass of particle k
n	Cell face normal vector
N	Number of phases
n_i	Number of particles in i phase
N_{ij}	Number of collisions between i and j particles
n	Number of particles
P	Particle stress or pressure tensor
P	Pressure
P_c	Collisional stress tensor
P_k	Kinetic stress tensor
$P_{k,i}$	Kinetic stress tensor of phase i
q_c	Collisional heat flux
q_k	Kinetic heat flux
r	Position vector
Re	Reynolds number
r_i	Radius of particle i
R_{ij}	Summation of the radius ($r_i + r_j$)
r_j	Radius of particle j
S	Source term
t	Time
v_i	Hydrodynamic mean velocity of i phase
v_j	Hydrodynamic mean velocity of j phase
V_p	Volume of particle
x_i	Arbitrary position of particle i.
x_j	Arbitrary position of particle j.

Greek Symbols

η	Kolmogorov length scale
θ	Granular temperature (old definition)
μ_s	Solid viscosity
$\mu_{col,s}$	Collisional part of solid viscosity
$\mu_{kin,s}$	Kinetic part of solid viscosity
$\mu_{dil,s}$	Dilute viscosity
ε	Volume fraction
ρ	Density
τ_s	Shear stress
β_{gs}	Drag coefficient between gas and solid
Γ	Diffusion coefficient
ω	Angular velocity
ζ_i	Bulk viscosity of phase I

References

1. Zhao, G.J.; Shi, X.G.; Wu, Y.Y.; Wang, M.; Zhang, M.X.; Gao, J.S.; Lan, X.Y. 3D CFD simulation of gas-solids hydrodynamics and bubbles behaviors in empty and packed bubbling fluidized beds. *Powder Technol.* **2019**, *351*, 1–15. [CrossRef]
2. Luo, Z.; Zhao, Y.; Lv, B.; Fu, Y.; Xu, X.; Chen, C. Dry coal beneficiation technique in the gas–solid fluidized bed: A review. *Int. J. Coal Prep. Util.* **2019**, *42*, 1–29. [CrossRef]
3. Rahaman, M.F.; Naser, J.; Witt, P.J. An unequal granular temperature kinetic theory: Description of granular flow with multiple particle classes. *Powder Technol.* **2003**, *138*, 82–92. [CrossRef]
4. Lv, B.; Luo, Z.; Fu, Y.; Zhang, B.; Qin, X.; Zhu, X. Particle mixing behavior of fine coal in density control of gas–solid separation fluidized bed. *Particuology* **2019**, *50*, 76–87. [CrossRef]
5. Fu, Z.; Zhu, J.; Barghi, S.; Zhao, Y.; Luo, Z.; Duan, C. The distribution of bed density in an air dense medium fluidized bed with single and binary mixtures of Geldart B and/or D particles. *Miner. Eng.* **2019**, *142*, 105926. [CrossRef]
6. Ostermeier, P.; Vandersickel, A.; Gleis, S.; Spliethoff, H. Numerical Approaches for Modeling Gas–Solid Fluidized Bed Reactors: Comparison of Models and Application to Different Technical Problems. *J. Energy Resour. Technol.* **2019**, *141*, 070707. [CrossRef]
7. Gidaspow, D.; Lu, H.L. Collisional viscosity of FCC particles in a CFB. *Aiche J.* **1996**, *42*, 2503–2510. [CrossRef]
8. Ding, J.; Gidaspow, D. A Bubbling Fluidization Model Using Kinetic-Theory of Granular Flow. *Aiche J.* **1990**, *36*, 523–538. [CrossRef]
9. Arastoopour, H.; Pakdel, P.; Adewumi, M. Hydrodynamic analysis of dilute gas—Solids flow in a vertical pipe. *Powder Technol.* **1990**, *62*, 163–170. [CrossRef]
10. Peng, L.; Wu, Y.; Wang, C.; Gao, J.; Lan, X. 2.5D CFD simulations of gas–solids flow in cylindrical CFB risers. *Powder Technol.* **2016**, *291*, 229–243. [CrossRef]
11. Zhou, Q.; Wang, J. CFD study of mixing and segregation in CFB risers: Extension of EMMS drag model to binary gas–solid flow. *Chem. Eng. Sci.* **2015**, *122*, 637–651. [CrossRef]
12. Wang, S.; Liu, G.D.; Lu, H.L.; Sun, L.Y.; Xu, P.F. CFD simulation of bubbling fluidized beds using kinetic theory of rough sphere. *Chem. Eng. Sci.* **2012**, *71*, 185–201. [CrossRef]
13. Lun, C.K.K.; Savage, S.B.; Jeffrey, D.J.; Chepurniy, N. Kinetic theories for granular flow: Inelastic particles in Couette flow and slightly inelastic particles in a general flowfield. *J. Fluid Mech.* **1984**, *140*, 223–256. [CrossRef]
14. Jenkins, J.T.; Savage, S.B. A theory for the rapid flow of identical, smooth, nearly elastic, spherical particles. *J. Fluid Mech.* **1983**, *130*, 187–202. [CrossRef]
15. Yang, L.; Padding, J.T.; Kuipers, J.A.M. Modification of kinetic theory of granular flow for frictional spheres, Part I: Two-fluid model derivation and numerical implementation. *Chem. Eng. Sci.* **2016**, *152*, 767–782. [CrossRef]
16. Gidaspow, D. *Multiphase Flow and Fluidization: Continuum and Kinetic Theory Descriptions*; Academic Press: Cambridge, MA, USA, 2012.
17. Manger, E. Modelling and Simulation of Gas/Solids Flow in Curvilinear Co ordinates. Ph.D. Thesis, Norwegian University of Science and Technology, Trondheim, Norway, 1996.
18. Bell, R.A. *Numerical Modelling of Multi-Particle Flows in Bubbling Gas-Solid Fluidized Beds*; Swinburne University of Technology: Melbourne City, Australia, 2000.
19. Huilin, L.; Wenti, L.; Rushan, B.; Lidan, Y.; Gidaspow, D. Kinetic theory of fluidized binary granular mixtures with unequal granular temperature. *Phys. A Stat. Mech. Its Appl.* **2000**, *284*, 265–276. [CrossRef]
20. Mathiesen, V.; Solberg, T.; Hjertager, B.H. An experimental and computational study of multiphase flow behavior in a circulating fluidized bed. *Int. J. Multiph. Flow* **2000**, *26*, 387–419. [CrossRef]
21. Dodds, D.; Sarhan, A.R.; Naser, J. CFD Investigation into the Effects of Surrounding Particle Location on the Drag Coefficient. *Fluids* **2022**, *7*, 331. [CrossRef]
22. Weaver, D.S.; Mišković, S. An Analysis of CFD-DEM with Coarse Graining for Turbulent Particle-Laden Jet Flows. *Fluids* **2023**, *8*, 215. [CrossRef]

23. Wang, S.; Luo, K.; Hu, C.S.; Sun, L.Y.; Fan, J.R. Effect of superficial gas velocity on solid behaviors in a full-loop CFB. *Powder Technol.* **2018**, *333*, 91–105. [CrossRef]
24. Zhang, W.; You, C.F. Numerical simulation of particulate flows in CFB riser with drag corrections based on particle distribution characterization. *Chem. Eng. J.* **2016**, *303*, 145–155. [CrossRef]
25. Wang, Q.; Niemi, T.; Peltola, J.; Kallio, S.; Yang, H.; Lu, J.; Wei, L. Particle size distribution in CPFD modeling of gas–solid flows in a CFB riser. *Particuology* **2015**, *21*, 107–117. [CrossRef]
26. Rossbach, V.; Utzig, J.; Decker, R.K.; Noriler, D.; Meier, H.F. Numerical gas-solid flow analysis of ring-baffled risers. *Powder Technol.* **2016**, *297*, 320–329. [CrossRef]
27. Wu, J.; Binbo, J.; Chen, J.; Yang, Y. Multi-scale study of particle flow in silos. *Adv. Powder Technol.* **2009**, *20*, 62–73. [CrossRef]
28. Miin, C.S.; Sulaiman, S.A.; Raghavan, V.R.; Heikal, M.R.; Naz, M.Y. Hydrodynamics of multi-sized particles in stable regime of a swirling bed. *Korean J. Chem. Eng.* **2015**, *32*, 2361–2367. [CrossRef]
29. Zheng, N.; Liu, H.; Fang, J.; Wei, J. Numerical investigation of bed-to-tube heat transfer in a shallow fluidized bed containing mixed-size particles. *Int. J. Heat Mass Transf.* **2023**, *211*, 124252. [CrossRef]
30. Mathiesen, V. *An Experimental and computational Study of Multiphase Flow Behavior in Circulating Fluidized Beds*; Telemark Institute of Technology: Notodden, Norway, 1997.
31. Rahaman, M.F.; Sarhan, A.R.; Naser, J. Kinetic theory for multi-particulate flow: Description of granular flow with rotary movement of particles. *Powder Technol.* **2020**, *360*, 780–788. [CrossRef]
32. Abramov, R.V. Turbulence via Intermolecular Potential: Viscosity and Transition Range of the Reynolds Number. *Fluids* **2023**, *8*, 101. [CrossRef]
33. Witt, P.J.; Perry, J.H.; Schwarz, M.P. A numerical model for predicting bubble formation in a 3D fluidized bed. *Appl. Math. Model.* **1998**, *22*, 1071–1080. [CrossRef]
34. Van Wachem, B.G.M.; Schouten, J.C.; van den Bleek, C.M.; Krishna, R.; Sinclair, J.L. Comparative analysis of CFD models of dense gas–solid systems. *Aiche J.* **2001**, *47*, 1035–1051. [CrossRef]
35. Tsuo, Y.P.; Gidaspow, D. Computation of Flow Patterns in Circulating Fluidized-Beds. *Aiche J.* **1990**, *36*, 885–896. [CrossRef]
36. Sobieski, W. Drag Coefficient in Solid–Fluid System Modeling with the Eulerian Multiphase Model. *Dry. Technol.* **2011**, *29*, 111–125. [CrossRef]
37. Zhang, Y.F.; Arastoopour, H. Dilute Fluidized Cracking Catalyst Particles—Gas-Flow Behavior in the Riser of a Circulating Fluidized-Bed. *Powder Technol.* **1995**, *84*, 221–229. [CrossRef]
38. Miller, A.; Gidaspow, D. Dense, Vertical Gas-Solid Flow in a Pipe. *Aiche J.* **1992**, *38*, 1801–1815. [CrossRef]
39. Farrell, M.; Lun, C.K.K.; Savage, S.B. A simple kinetic theory for granular flow of binary mixtures of smooth, inelastic, spherical particles. *Acta Mech.* **1986**, *63*, 45–60. [CrossRef]
40. Jenkins, J.T.; Mancini, F. Balance Laws and Constitutive Relations for Plane Flows of a Dense, Binary Mixture of Smooth, Nearly Elastic, Circular Disks. *J. Appl. Mech. T ASME* **1987**, *54*, 27–34. [CrossRef]